

Article

In Silico Molecular Study of Tryptophan Bitterness

Antonella Di Pizio *  and Alessandro Nicoli 

Leibniz-Institute for Food Systems Biology at the Technical University of Munich, Lise-Meitner-Str. 34, 85354 Freising, Germany; a.nicoli.leibniz-lsb@tum.de

* Correspondence: a.dipizio.leibniz-lsb@tum.de; Tel.: +49-816-171-6516

Academic Editor: Panagiotis Zoumpoulakis

Received: 20 August 2020; Accepted: 7 October 2020; Published: 11 October 2020



Abstract: Tryptophan is an essential amino acid, required for the production of serotonin. It is the most bitter amino acid and its bitterness was found to be mediated by the bitter taste receptor TAS2R4. Di-tryptophan has a different selectivity profile and was found to activate three bitter taste receptors, whereas tri-tryptophan activated five TAS2Rs. In this work, the selectivity/promiscuity profiles of the mono-to-tri-tryptophans were explored using molecular modeling simulations to provide new insights into the molecular recognition of the bitter tryptophan. Tryptophan epitopes were found in all five peptide-sensitive TAS2Rs and the best tryptophan epitope was identified and characterized at the core of the orthosteric binding site of TAS2R4.

Keywords: TAS2Rs; GPCRs; amino acids; homology modeling; docking

1. Introduction

Tryptophan (three-letter code: Trp, one-letter code: W) is one of the nine essential, or indispensable, amino acids. It is required for the production of serotonin and therefore has an important role in many fundamental physiological functions such as sleep, mood, cognition, and behavior [1–3]. It is a key component in the human diet. Nutritional tryptophan-containing supplements proved to be highly beneficial in malnutrition and undernutrition states, derived often by certain pathological conditions [4]. Due to its role in the serotonin pathway, tryptophan levels are affected in the course of metabolic disorders, and tryptophan supplements are associated with the medical treatment of several diseases such as depression, sleep disorders, cognitive disorders, anxiety, or neurodegenerative diseases [5].

Among the free amino acids, tryptophan has the lowest bitter taste threshold (BTT: 4 mmol/L) [6]. The bitter taste of tryptophan can lead to a reduction in the consumption of tryptophan-based nutritional supplements [7]. To gain from their effect, patients must consume the prescribed amount of supplements for the recommended time, but sensory characteristics strongly affect the patients' acceptability and the correct assumption of nutritional supplements [8].

In humans, the bitter taste is mediated by a repertoire of 25 bitter taste receptors (TAS2Rs) [9–11], representing a separate branch usually associated with class A G protein-coupled receptors (GPCRs) [12,13]. The recognition of bitter molecules is complex: bitter compounds can activate selectively one TAS2R or several receptors promiscuously [14].

Although essential branched amino acids trigger generally aversive bitter taste perception [6,15], very few studies focused on their molecular recognition by bitter taste receptors. The bitter taste of amino acids and peptides was found to be mediated by a pattern of five peptide-sensitive TAS2Rs (i.e., TAS2R1, -R4, -R14, -R39, -R46) [16]. Tryptophan (W) selectively activates, with limited potency, the bitter taste receptor TAS2R4, whereas di-tryptophan (WW) and tri-tryptophan (WWW) exhibit considerable increases in the potencies and recruitment of additional receptors, with the tri-tryptophan activating all peptide-sensitive TAS2Rs (Table 1) [16].

Table 1. Glide SP scores (kcal/mol) of mono-to-tri-tryptophans docked into peptide-sensitive TAS2Rs. Activity values (threshold and EC₅₀ when available) of TAS2Rs activated by mono-to-tri-tryptophans, as determined by Kohl et al. 2013 [16]. Cells are colored in green when the peptide was found to be active with the calcium-imaging assay and in red if potency could not be determined.

		TAS2R4	TAS2R1	TAS2R39	TAS2R14	TAS2R46
WWW	Activity (mM)	0.01 (EC ₅₀ : 0.03 ± 0.005)	0.1	0.1	0.1	0.1
	Glide score	−10.88	−8.82	−8.10	−8.48	−8.20
WW	Activity (mM)	1.0 (EC ₅₀ : 0.66 ± 0.03)	0.3	1.0		
	Glide score	−8.59	−8.71	−8.35	−5.55	−5.27
W	Activity (mM)	10				
	Glide score	−7.05	−5.36	−5.34	−5.43	−5.05

In this study, we used *in silico* methods to investigate the binding modes of this little series of tryptophan-containing peptides and then, by the comparison of the obtained poses, to gain insights into the molecular recognition of the bitter tryptophan. Understanding the molecular mechanisms leading to the unpleasant bitter taste of the tryptophan may lead to the development of new strategies to ensure the acceptability of tryptophan-containing supplements. Moreover, bitter taste receptors are also expressed in extra-oral tissues such as in the hearth, in the brain, and in the gastrointestinal tract [17]. Therefore, investigations of the interaction of TAS2Rs with amino acids and peptides can help shed light on the function of the ‘ecnomotopically’ [18] expressed TAS2Rs, whose endogenous ligands are not known yet, but peptides are definitely good candidates.

2. Results

Despite the recent advancements in GPCR structural biology, no TAS2R experimental structure is currently available and computational techniques are currently used to predict the binding modes of bitter compounds, both small molecules [19] and amino acids/peptides [20–22], into their cognate TAS2Rs. The orthosteric binding site of TAS2Rs was found to coincide with that of class A GPCRs and the multi-specificity of bitter compounds was achieved by using sub-pockets within the orthosteric binding site, allowing for different types of interactions for different ligands [12,23–25].

The five peptide-sensitive TAS2Rs (i.e., TAS2R1, -R4, -R14, -R39, -R46) share low sequence identity among them and this difference is even more pronounced in the binding site (Supplementary Material Figure S1). Here, structural models of all peptide-sensitive TAS2R binding sites were used to characterize the selectivity/promiscuity profiles of mono-to-tri-tryptophans and to identify the putative binding mode of tryptophan.

2.1. From the Promiscuous Tri-Tryptophan to the Selective Tryptophan

Tri-tryptophan is the most promiscuous of the analyzed compounds. According to the performed docking studies, it fills in the binding site of the three peptide-sensitive bitter taste receptors in a highly complementary manner, as quantified by Glide Standard Precision (SP) score values that were below −8 kcal/mol in all cases (Table 1). Docking scores in general [26], and Glide scores in particular [27,28], have been successfully used for capturing the main ligand-receptor interactions and comparing binding modes. Glide SP scores, used here as an approximation of the binding affinity, were in good agreement with the experimental data: lower binding energy (lower Glide SP score) was indeed observed for tri-tryptophan in complex with TAS2R4 (experimental EC₅₀: 0.03 mM) than in complex with the other receptors (experimental threshold values of 0.1 mM) (Table 1).

To better understand the predicted affinity difference of the tri-tryptophan toward the different receptors, we analyzed the docking poses of the di-tryptophan, which resulted in activating TAS2R4, -R1, and -R39, but not TAS2R14 and -R46. Comparing the binding modes of tri-tryptophan and

di-tryptophan, we noticed that the contribution of the third residue to the binding was different for the different receptors. Di-tryptophan (WW) and tri-tryptophan (WWW) had very similar Glide SP scores when docked into the binding sites of TAS2R1 and -R39, which suggests that the interaction of the third tryptophan residue (colored in magenta in Figure 1A) does not have a relevant contribution to the binding. Differently, within the TAS2R4 binding site, the third tryptophan residue was predicted to increase the affinity of the tri-tryptophan compared to the di-tryptophan of $-2-29$ kcal/mol. According to the docking analysis, only the tri-tryptophan, with its flexibility and bigger size, could ensure a good fitting within the binding sites of TAS2R14 and -R46, and the inactive di-tryptophan was predicted as a weak binder (Glide SP scores of -5.55 and -5.27 kcal/mol, respectively). Experimental data suggest that also the second tryptophan residue does not help gain potency toward TAS2R14 and -R46, since the single tryptophan is inactive toward these two receptors. In contrast, the second tryptophan residue results were determinant to elicit receptor activation for TAS2R1 and -R39.

Comparing the predicted binding modes of di-tryptophan (WW) and tryptophan (W), we could evaluate the contribution of the second tryptophan residue and therefore which of the sub-pockets identified for the tri- and di-tryptophans were the best tryptophan epitopes in each peptide-sensitive TAS2R (Figure 1C). The Glide SP score of the tryptophan into TAS2R14 and -R46 was high and comparable to that of the di-tryptophan. We also found low Glide SP scores for the tryptophan in complex with TAS2R1 and -R39, and this can be an explanation of the experimental results, which showed that one single tryptophan residue is not sufficient to lead to the receptor activation of TAS2R1 and -R39.

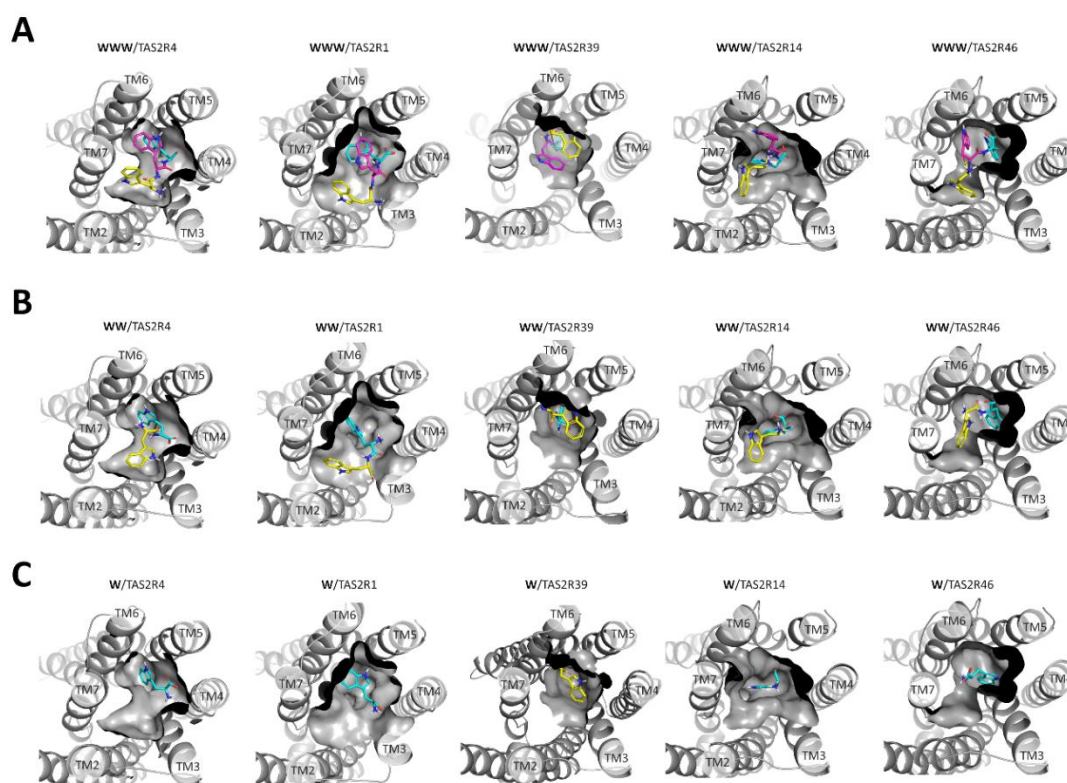


Figure 1. Predicted binding modes of tri-tryptophan (A), di-tryptophan (B), and tryptophan (C) into the binding sites of TAS2R4, -R1, -R39, -R14, and -R46. The receptors are shown in the same orientation in all representations. Tryptophan residues are colored in cyan when accommodated at the bottom of the orthosteric binding site, in magenta when close to the extracellular space, and in yellow when in between. Receptor sub-pockets are shown in Supplementary Material Figure S2.

2.2. Predicted Binding Mode of Tryptophan into TAS2R4

The docking results of the tri-tryptophan into the five peptide-sensitive TAS2Rs revealed the sub-pockets accommodating tryptophan residues in each receptor (all tryptophan epitopes are shown in Supplementary Material Figure S2). The binding of tryptophan residues to the individual epitopes had different affinities. Of all five peptide-sensitive receptors, only TAS2R4 could be activated by the tryptophan, and therefore this should contain the best tryptophan epitope. Among the docking poses of the tryptophan into the three identified TAS2R4 epitopes (Figure S2A), the highest score was obtained for a pose located at the core of the orthosteric binding site (epitope 1). The tryptophan was predicted to establish a π - π interaction with Tyr242^{6.51} and an H-bond with Thr246^{6.55} (Figures 2A and 3A). Residue superscript numbering indicates Ballesteros–Weinstein (BW) positions and makes the comparison easier of the transmembrane positions with other TAS2Rs and class A GPCRs [13,29]. The interactions between the tryptophan and the residues Tyr242^{6.51} and Thr246^{6.55} were predicted to be maintained for di-tryptophan and tri-tryptophan, whereas the additional tryptophan residues were accommodated by other sub-pockets (Figure 1, Figures S2 and S3).

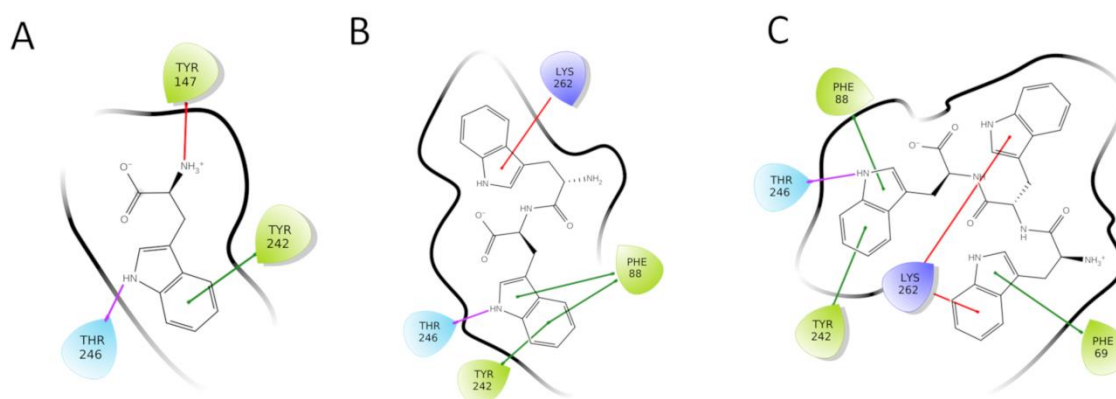


Figure 2. 2D representations of the interactions established by tryptophan (A), di-tryptophan (B), and tri-tryptophan (C) within the TAS2R4 orthosteric binding site. H-bonds, π - π interactions, and π -cation interactions are represented as magenta, green, and red lines, respectively.

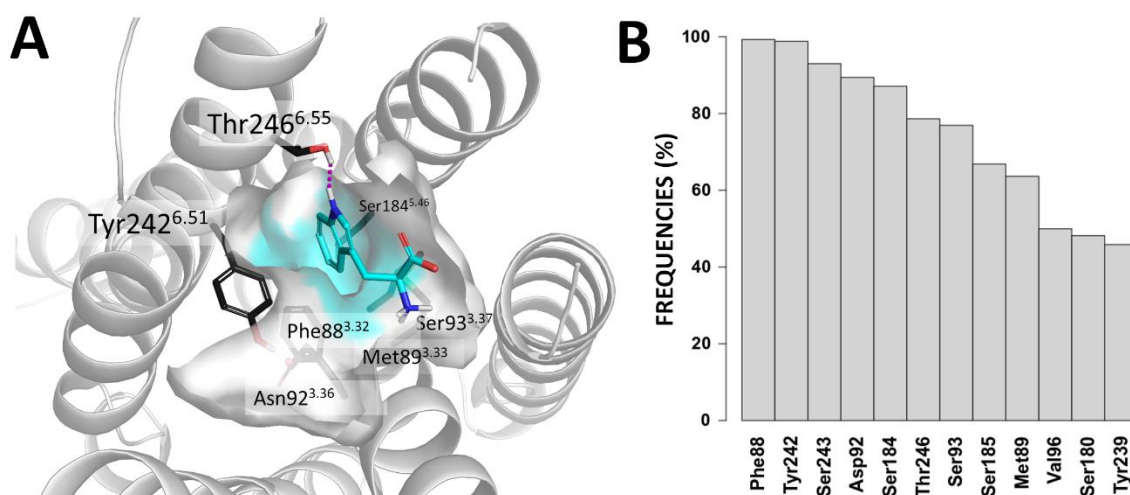


Figure 3. (A) Docking pose of the tryptophan within TAS2R4 epitope 1. The surface of the epitope is colored in cyan. Residues involved in shaping the epitope are shown as dark grey sticks. Tryptophan is represented as cyan sticks. The H-bond between the ligand and Thr246^{6.55} is shown as a magenta dashed line. (B) Frequencies of the contacts between the tryptophan with TAS2R4 residues during the MD simulation.

The resulting docking poses of tryptophan, di-tryptophan, and tri-tryptophan into TAS2R4 were submitted to post-docking Molecular Dynamics (MD) simulations of 20 ns. The root-mean-square deviation (RMSD) analyses indicated that, within the simulated time, the ligand positions did not deviate from the starting docking poses and, signally, the ligand indole moieties were very stable in their position within the identified TAS2R4 epitopes (Supplementary Material Figures S4 and S5).

In Figure 3, we report the 3D representation of the TAS2R4 epitope accommodating the tryptophan and the frequencies of contacts between tryptophan and TAS2R4, which were found during the post-docking MD simulation. Residues shaping this subpocket (Phe88^{3.32}, Met89^{3.33}, Asp92^{3.36}, Ser93^{3.37}, Ser184^{5.46}, Tyr242^{6.51}, Thr246^{6.55}) were indeed among the residues found to be mostly involved in the binding process during the MD simulations.

3. Discussion

The tryptophan bitter taste was found to be mediated by TAS2R4 [16], but, to the best of our knowledge, the interaction of this relevant amino acid with the cognate bitter taste receptor has not been investigated. Interestingly, di-tryptophan and tri-tryptophan showed increased potency toward TAS2R4 and activate additional TAS2R members (Table 1). Therefore, tryptophan (W), di-tryptophan (WW), and tri-tryptophan (WWW) constitute an interesting case study to investigate structure–activity relationships into the bitter taste receptors and to characterize the molecular determinants leading to the tryptophan bitter taste.

We identified the sub-pockets accommodating the tryptophan in the orthosteric binding sites of the five peptide-sensitive bitter taste receptors and we found that these tryptophan epitopes are located in different regions of the receptors (Supplementary Material Figure S2). This also suggests that for peptides, as previously found for small molecules [12,23–25], the determinants for activation are receptor-specific. Moreover, the interaction of individual tryptophan residues with individual epitopes has a different contribution to the overall binding energy of the promiscuous tri-tryptophan, explaining the selectivity profile of the analyzed molecules against the five peptide-sensitive TAS2Rs.

Comparing the docking poses and Glide scores of the mono-to-tri-tryptophans, we unraveled the putative binding mode of tryptophan within the TAS2R4 binding site. The identified binding pose was highly scored (Glide SP score -7.05 kcal/mol) and resulted in being rather stable during the post-docking MD simulation. Tryptophan was surrounded by numerous hydrophobic/aromatic residues (Phe88^{3.32}, Met89^{3.33}, Tyr242^{6.51}) and was predicted to interact with Tyr242^{6.51} and Thr246^{6.55} through π – π and H-bond interactions, respectively. Both BW positions 6.51 [23,24,30–33] and 6.55 [30,31,34] were previously indicated as agonist-interacting positions in other bitter taste receptors. Moreover, these interactions are indeed predicted to be maintained for di-tryptophan and tri-tryptophan (Figure 2), suggesting that the sub-pocket around Phe88^{3.32} and Tyr242^{6.51} is the best epitope for the recognition of tryptophan by TAS2R4 (TAS2R4 epitope 1, Figures S2A and S3A).

4. Materials and Methods

Homology modeling. Structural models of TAS2R1, -R14, and -R46 were generated in previous works [28,30,35]. The TAS2R14 receptor model was then used here as a template for modeling the initial structures of TAS2R4 and -R39. These structures were then refined by performing induced-fit simulations (Schrödinger Suite 2018-3 Induced Fit Docking protocol; Glide, Schrödinger, LLC, New York, NY, USA, 2016; Prime, Schrödinger, LLC, New York, NY, 2018) [36] with the most potent known ligand (i.e., TAS2R4 with quinine (EC₅₀: 600 μ M, activity threshold 10 μ M [37,38]) and TAS2R39 with genistein (EC₅₀: 50 μ M [39]), predicted binding poses are shown in Supplementary Material, Figures S6 and S7). Docking was performed with the Glide Standard Precision (SP) accuracy level. The receptor conformation that gave the lowest Glide score was selected for the following docking studies.

Peptide docking. 3D structures of the analyzed amino acid and peptides were built with the “Build Peptide from Sequence” tool available in Maestro 11.7 and prepared for docking through the generation

of protonation states at pH 7 ± 1.0 with LigPrep, as implemented in the Schrödinger Small-Molecule Drug Discovery Suite 2018-3 (Schrödinger, LLC, New York, NY, USA, 2018). Glide software (version 8.2, Schrödinger, LLC, New York, NY, USA, 2018) was used for docking the tryptophan, di-tryptophan, and tri-tryptophan to the peptide-sensitive TAS2R models. The grid box of all analyzed receptors was centroid of the main chains of the binding site residues (BW positions: 2.61, 3.29, 3.32, 3.36, 4.64, 5.35, 5.38, 5.39, 5.42, 5.46, 6.51, 6.55, and 7.39), using the option “Generate grid suitable for peptide docking” and allowing rotation of the binding site hydroxyl and thiol groups. The docking was then performed with the SP-peptide mode of Glide, which was specifically developed for the accurate prediction of binding complex geometries of peptides to receptors [40]. Docking poses of tri-tryptophan with the lowest Glide scores were then used as a selection filter for the docking poses of di-tryptophan and tri-tryptophan for each analyzed TAS2R: we considered the poses with the lowest scores among poses that reproduce the binding of one of the tripeptide residues. The Glide SP scores and ligand efficiency values of all selected poses are reported in Table 1 and Table S1, respectively. To provide additional score values for the identified binding modes, we applied the MM-GBSA scoring (Prime, Schrödinger, LLC, New York, NY, USA, 2018) of each of the predicted poses (Supplementary Material Table S2).

2D representations of the peptides/TAS2R4 binding modes (as reported in Figure 3 and Figure S3) were generated with the “Ligand Interaction Diagram” tool available in Maestro 11.7 (Schrödinger, LLC, New York, NY, USA, 2018).

Post-docking Molecular Dynamics (MD) simulations. The coordinates of the analyzed ligands in complex with TAS2R4 were embedded into a 1-palmitoyl-2-oleyl-sn-glycerol-3-phosphocholine (POPC) bilayer of $90 \times 90 \text{ \AA}$ using VMD Membrane Builder Plugin Tool [41]. The orientation of the TAS2R4 homology model within the membrane bilayer was obtained from the coordinates of the $\beta 2$ adrenergic receptor (PDB ID: 3SN6), as deposited in the Orientations of Proteins in Membranes (OPM) database [42]. Overlapping lipids (within 0.55 \AA) were removed upon protein insertion, and the systems were solvated with TIP3P water molecules at 15 \AA from protein atoms using VMD Solvate plugin 1.5 and neutralized by Na^+/Cl^- to reach a final physiological concentration of 0.154 M by using VMD Autonize plugin 1.3 [41,43].

All MD simulations with periodic boundary conditions were carried out with ACEMD (Acellera, version 3.2) [44] using the CHARMM36 force field [45,46]. The systems were equilibrated through a 2000 conjugate gradient step minimization, followed by 20 ns of MD simulation in the NPT ensemble by applying initial constrains that were gradually reduced (positional constraints of $5 \text{ kcal}\cdot\text{mol}^{-1}\cdot\text{\AA}^{-2}$ on ligand, protein, and lipid phosphor atoms in the first 5 ns, positional constraints of $5 \text{ kcal}\cdot\text{mol}^{-1}\cdot\text{\AA}^{-2}$ on ligand and protein atoms in the following 10 ns, positional constraints of $5 \text{ kcal}\cdot\text{mol}^{-1}\cdot\text{\AA}^{-2}$ on ligand atoms and protein $\text{C}\alpha$ atoms in the last 5 ns). During the equilibration, the temperature was maintained at 310 K using a Langevin thermostat with a low damping constant of 1 ps^{-1} , and the pressure was maintained at 1 atm using a Berendensen barostat. The M-SHAKE algorithm [47,48] was used to constrain the bond lengths involving hydrogen atoms. The equilibrated systems were then subjected to 20 ns of the unrestrained MD simulation run (NVT ensemble, timestep = 2 fs , $T = 310 \text{ K}$, damping constant = 0.1 ps^{-1}). Long-range Coulombic interactions were handled using the particle mesh Ewald summation method (PME) [49] with a grid size rounded to the approximate integer value of the cell wall dimensions. A non-bonded cutoff distance of 9 \AA with a switching distance of 7.5 \AA was used.

The number of contacts between the analyzed ligands (W, WW, WWW) and TAS2R4 was computed using the contactFreq.tcl script in VMD [41], setting a distance cut-off of 4 \AA . Root-mean-square deviations (RMSDs) to the docking poses were computed for ligand heavy atoms and ligand indole scaffold heavy atoms using ProDy [50]. The resulting interaction frequencies were plotted using Bar Plots in R.

5. Conclusions

Tryptophan is an essential amino acid, required for the production of serotonin. It is the most bitter amino acid and its bitterness was found to be mediated by the bitter taste receptor TAS2R4 [16]. In this work, we analyzed the putative interaction of tryptophan, di-tryptophan and tri-tryptophan into the cognate bitter taste receptors. Combining comparative modeling, docking, and MD investigations allowed us (i) to rationalize the factors contributing to improving the activity values toward individual TAS2Rs while growing the peptide chain; (ii) to investigate the selectivity/promiscuity profile of the five peptide-sensitive TAS2Rs toward analyzed tryptophan peptides; and (iii) to identify and characterize the best tryptophan epitope.

Supplementary Materials: Supplementary materials are available online, Figure S1: Sequence alignment of analyzed TAS2Rs, Figure S2. Tryptophan epitopes in the orthosteric binding sites of TAS2R4, TAS2R1, TAS2R39, TAS2R14, TAS2R46. Figure S3. 2D representations of the interactions established by tryptophan, di-tryptophan, and tri-tryptophan within the orthosteric binding site of TAS2R1, TAS2R39, TAS2R14, TAS2R46. Figure S4. RMSD plots of ligand heavy atoms through 20ns MD of tryptophan/TAS2R4, di-tryptophan/TAS2R4, and tri-tryptophan/TAS2R4. Figure S5. RMSD plots of ligands' indole moieties through 20 ns MD. Figure S6. Predicted binding mode of quinine within the TAS2R4 orthosteric binding site. Figure S7. Predicted binding mode of quinine within the TAS2R39 orthosteric binding site. Table S1: Ligand Efficiency (LE) values, as calculated by docking simulations of mono-to-tri-tryptophans towards peptide-sensitive TAS2Rs. Table S2: MM-GBSA dG bind values calculated with Prime.

Author Contributions: Conceptualization, Writing the original draft, A.D.P. Investigation, Writing—review and editing, A.D.P. and A.N. All authors have read and agreed to the published version of the manuscript.

Funding: This work was supported by the Technical University of Munich in the framework of the Open Access Publishing Program.

Acknowledgments: The authors thank Stefano Moro and the Molecular Modeling Section, University of Padua (Italy), and Giuseppe Deganutti, Coventry University (UK), for insightful suggestions on the MD protocol. A.D.P. participates in the European COST Actions CA18133 (ERNEST) and CA15118 (FoodMC).

Conflicts of Interest: The authors declare no conflict of interest.

References

1. Jenkins, T.A.; Nguyen, J.C.; Polglaze, K.E.; Bertrand, P.P. Influence of tryptophan and serotonin on mood and cognition with a possible role of the gut-brain axis. *Nutrients* **2016**, *8*, 56. [[CrossRef](#)] [[PubMed](#)]
2. Richard, D.M.; Dawes, M.A.; Mathias, C.W.; Acheson, A.; Hill-Kapturczak, N.; Dougherty, D.M. L-Tryptophan: Basic metabolic functions, behavioral research and therapeutic indications. *Int. J. Tryptophan Res.* **2009**, *2*, 45–60. [[CrossRef](#)] [[PubMed](#)]
3. Kaluzna-Czaplinska, J.; Gaterek, P.; Chirumbolo, S.; Chartrand, M.S.; Bjorklund, G. How important is tryptophan in human health? *Crit. Rev. Food Sci.* **2019**, *59*, 72–88. [[CrossRef](#)] [[PubMed](#)]
4. Nikolaus, S.; Schulte, B.; Al-Massad, N.; Thieme, F.; Schulte, D.M.; Bethge, J.; Rehman, A.; Tran, F.; Aden, K.; Hasler, R.; et al. Increased tryptophan metabolism is associated with activity of inflammatory bowel diseases. *Gastroenterology* **2017**, *153*, 1504–1516. [[CrossRef](#)] [[PubMed](#)]
5. Comai, S.; Bertazzo, A.; Brughera, M.; Crotti, S. Tryptophan in health and disease. *Adv. Clin. Chem.* **2020**, *95*, 165–218. [[CrossRef](#)] [[PubMed](#)]
6. Wieser, H.; Belitz, H.D. Relations between structure and bitter taste of amino-acids and peptides. 1. Amino-acids and related compounds. *Z. Lebensm.-Unters. Forsch.* **1975**, *159*, 65–72. [[CrossRef](#)]
7. Drewnowski, A.; Gomez-Carneros, C. Bitter taste, phytonutrients, and the consumer: A review. *Am. J. Clin. Nutr.* **2000**, *72*, 1424–1435. [[CrossRef](#)]
8. Delompre, T.; Guichard, E.; Briand, L.; Salles, C. Taste perception of nutrients found in nutritional supplements: A review. *Nutrients* **2019**, *11*, 2050. [[CrossRef](#)]
9. Adler, E.; Hoon, M.A.; Mueller, K.L.; Chandrashekar, J.; Ryba, N.J.; Zuker, C.S. A novel family of mammalian taste receptors. *Cell* **2000**, *100*, 693–702. [[CrossRef](#)]
10. Chandrashekar, J.; Mueller, K.L.; Hoon, M.A.; Adler, E.; Feng, L.X.; Guo, W.; Zuker, C.S.; Ryba, N.J.P. T2Rs function as bitter taste receptors. *Cell* **2000**, *100*, 703–711. [[CrossRef](#)]

11. Matsunami, H.; Montmayeur, J.P.; Buck, L.B. A family of candidate taste receptors in human and mouse. *Nature* **2000**, *404*, 601–604. [[CrossRef](#)] [[PubMed](#)]
12. Di Pizio, A.; Niv, M.Y. Computational Studies of Smell and Taste Receptors. *Isr. J. Chem.* **2014**, *54*, 1205–1218. [[CrossRef](#)]
13. Di Pizio, A.; Levit, A.; Slutzki, M.; Behrens, M.; Karaman, R.; Niv, M.Y. Comparing Class A GPCRs to bitter taste receptors: Structural motifs, ligand interactions and agonist-to-antagonist ratios. *Method Cell Biol.* **2016**, *132*, 401–427. [[CrossRef](#)]
14. Di Pizio, A.; Niv, M.Y. Promiscuity and selectivity of bitter molecules and their receptors. *Bioorgan. Med. Chem.* **2015**, *23*, 4082–4091. [[CrossRef](#)]
15. Toelstede, S.; Hofmann, T. Quantitative studies and taste re-engineering experiments toward the decoding of the nonvolatile sensometabolome of Gouda cheese. *J. Agr. Food Chem.* **2008**, *56*, 5299–5307. [[CrossRef](#)]
16. Kohl, S.; Behrens, M.; Dunkel, A.; Hofmann, T.; Meyerhof, W. Amino acids and peptides activate at least five members of the human bitter taste receptor family. *J. Agr. Food Chem.* **2013**, *61*, 53–60. [[CrossRef](#)]
17. Lee, S.J.; Depoortere, I.; Hatt, H. Therapeutic potential of ectopic olfactory and taste receptors. *Nat. Rev. Drug Discov.* **2019**, *18*, 116–138. [[CrossRef](#)]
18. Di Pizio, A.; Behrens, M.; Krautwurst, D. Beyond the Flavour: The Potential Druggability of Chemosensory G Protein-Coupled Receptors. *Int. J. Mol. Sci.* **2019**, *20*, 1402. [[CrossRef](#)]
19. Spaggiari, G.; Di Pizio, A.; Cozzini, P. Sweet, umami and bitter taste receptors: State of the art of in silico molecular modeling approaches. *Trends Food Sci. Tech.* **2020**, *96*, 21–29. [[CrossRef](#)]
20. Upadhyaya, J.; Pydi, S.P.; Singh, N.; Aluko, R.E.; Chelikani, P. Bitter taste receptor T2R1 is activated by dipeptides and tripeptides. *Biochem. Bioph. Res. Commun.* **2010**, *398*, 331–335. [[CrossRef](#)]
21. Dai, W.M.; You, Z.L.; Zhou, H.; Zhang, J.; Hu, Y.Q. Structure-function relationships of the human bitter taste receptor hTAS2R1: Insights from molecular modeling studies. *J. Recept. Signal Transduct.* **2011**, *31*, 229–240. [[CrossRef](#)] [[PubMed](#)]
22. Stoeger, V.; Holik, A.K.; Holz, K.; Dingjan, T.; Hans, J.; Ley, J.P.; Krammer, G.E.; Niv, M.Y.; Somoza, M.M.; Somoza, V. Bitter-tasting amino acids l-arginine and l-isoleucine differentially regulate proton secretion via t2r1 signaling in human parietal cells in culture. *J. Agr. Food Chem.* **2020**, *68*, 3434–3444. [[CrossRef](#)] [[PubMed](#)]
23. Born, S.; Levit, A.; Niv, M.Y.; Meyerhof, W.; Behrens, M. The human bitter taste receptor TAS2R10 is tailored to accommodate numerous diverse ligands. *J. Neurosci.* **2013**, *33*, 201–213. [[CrossRef](#)] [[PubMed](#)]
24. Brockhoff, A.; Behrens, M.; Niv, M.Y.; Meyerhof, W. Structural requirements of bitter taste receptor activation. *Proc. Natl. Acad. Sci. USA* **2010**, *107*, 11110–11115. [[CrossRef](#)]
25. Nowak, S.; Di Pizio, A.; Levit, A.; Niv, M.Y.; Meyerhof, W.; Behrens, M. Reengineering the ligand sensitivity of the broadly tuned human bitter taste receptor TAS2R14. *Biochim. Biophys. Acta Gen. Subj.* **2018**, *1862*, 2162–2173. [[CrossRef](#)]
26. Shoichet, B.K.; Kobilka, B.K. Structure-based drug screening for G-protein-coupled receptors. *Trends Pharmacol. Sci.* **2012**, *33*, 268–272. [[CrossRef](#)]
27. Di Pizio, A.; Kruetzfeldt, L.M.; Cheled-Shoval, S.; Meyerhof, W.; Behrens, M.; Niv, M.Y. Ligand binding modes from low resolution GPCR models and mutagenesis: Chicken bitter taste receptor as a test-case. *Sci. Rep.* **2017**, *7*, 1–11. [[CrossRef](#)]
28. Di Pizio, A.; Waterloo, L.A.W.; Brox, R.; Lober, S.; Weikert, D.; Behrens, M.; Gmeiner, P.; Niv, M.Y. Rational design of agonists for bitter taste receptor TAS2R14: From modeling to bench and back. *Cell Mol. Life Sci.* **2019**, *77*, 531–542. [[CrossRef](#)]
29. Ballesteros, J.A.; Weinstein, H. Integrated methods for the construction of three-dimensional models and computational probing of structure-function relations in G protein-coupled receptors. *Methods Neurosci.* **1995**, *25*, 366–428.
30. Dunkel, A.; Hofmann, T.; Di Pizio, A. In silico investigation of bitter hop-derived compounds and their cognate bitter taste receptors. *J. Agric. Food Chem.* **2020**, *68*, 10414–10423. [[CrossRef](#)]
31. Sandal, M.; Behrens, M.; Brockhoff, A.; Musiani, F.; Giorgetti, A.; Carloni, P.; Meyerhof, W. Evidence for a transient additional ligand binding site in the tas2r46 bitter taste receptor. *J. Chem. Theory Comput.* **2015**, *11*, 4439–4449. [[CrossRef](#)] [[PubMed](#)]
32. Fierro, F.; Giorgetti, A.; Carloni, P.; Meyerhof, W.; Alfonso-Prieto, M. Dual binding mode of “bitter sugars” to their human bitter taste receptor target. *Sci. Rep.* **2019**, *9*, 1–16. [[CrossRef](#)] [[PubMed](#)]

33. Marchiori, A.; Capece, L.; Giorgetti, A.; Gasparini, P.; Behrens, M.; Carloni, P.; Meyerhof, W. Coarse-grained/molecular mechanics of the tas2r38 bitter taste receptor: Experimentally-validated detailed structural prediction of agonist binding. *PLoS ONE* **2013**, *8*. [[CrossRef](#)] [[PubMed](#)]
34. Sakurai, T.; Misaka, T.; Ishiguro, M.; Masuda, K.; Sugawara, T.; Ito, K.; Kobayashi, T.; Matsuo, S.; Ishimaru, Y.; Asakura, T.; et al. Characterization of the β -D-Glucopyranoside binding site of the human bitter taste receptor hTAS2R16. *J. Biol. Chem.* **2010**, *285*, 28373–28378. [[CrossRef](#)]
35. Xue, A.Y.; Di Pizio, A.; Levit, A.; Yarnitzky, T.; Penn, O.; Pupko, T.; Niv, M.Y. Independent evolution of strychnine recognition by bitter taste receptor subtypes. *Front. Mol. Biosci.* **2018**, *5*, 9. [[CrossRef](#)]
36. Sherman, W.; Day, T.; Jacobson, M.P.; Friesner, R.A.; Farid, R. Novel procedure for modeling ligand/receptor induced fit effects. *J. Med. Chem.* **2006**, *49*, 534–553. [[CrossRef](#)]
37. Pydi, S.P.; Sobotkiewicz, T.; Billakanti, R.; Bhullar, R.P.; Loewen, M.C.; Chelikani, P. Amino acid derivatives as bitter taste receptor (T2R) Blockers. *J. Biol. Chem.* **2014**, *289*, 25054–25066. [[CrossRef](#)]
38. Meyerhof, W.; Batram, C.; Kuhn, C.; Brockhoff, A.; Chudoba, E.; Bufer, B.; Appendino, G.; Behrens, M. The molecular receptive ranges of human tas2r bitter taste receptors. *Chem. Senses* **2010**, *35*, 157–170. [[CrossRef](#)]
39. Roland, W.S.U.; Vincken, J.P.; Gouka, R.J.; van Buren, L.; Gruppen, H.; Smit, G. Soy isoflavones and other isoflavonoids activate the human bitter taste receptors hTAS2R14 and hTAS2R39. *J. Agr. Food Chem.* **2011**, *59*, 11764–11771. [[CrossRef](#)]
40. Tubert-Brohman, I.; Sherman, W.; Repasky, M.; Beuming, T. Improved docking of polypeptides with Glide. *J. Chem. Inf. Modeling* **2013**, *53*, 1689–1699. [[CrossRef](#)]
41. Humphrey, W.; Dalke, A.; Schulten, K. VMD—Visual molecular dynamics. *J. Mol. Graph.* **1996**, *14*, 33–38. [[CrossRef](#)]
42. Lomize, M.A.; Lomize, A.L.; Pogozheva, I.D.; Mosberg, H.I. OPM: Orientations of proteins in membranes database. *Bioinformatics* **2006**, *22*, 623–625. [[CrossRef](#)] [[PubMed](#)]
43. Jorgensen, W.L.; Chandrasekhar, J.; Madura, J.D.; Impey, R.W.; Klein, M.L. Comparison of simple potential functions for simulating liquid water. *J. Chem. Phys.* **1983**, *79*, 926. [[CrossRef](#)]
44. Harvey, M.J.; Giupponi, G.; Fabritiis, G.D. ACEMD: Accelerating biomolecular dynamics in the microsecond time scale. *J. Chem. Theory Comput.* **2009**, *5*, 1632–1639. [[CrossRef](#)] [[PubMed](#)]
45. Huang, J.; MacKerell, A.D. CHARMM36 All-atom additive protein force field: Validation based on comparison to NMR data. *J. Comput. Chem.* **2013**, *34*, 2135–2145. [[CrossRef](#)]
46. Huang, J.; Rauscher, S.; Nawrocki, G.; Ran, T.; Feig, M.; de Groot, B.L.; Grubmüller, H.; MacKerell, A.D. CHARMM36m: An improved force field for folded and intrinsically disordered proteins. *Nat. Methods* **2017**, *14*, 71–73. [[CrossRef](#)]
47. Forester, T.R.; Smith, W. SHAKE, rattle and roll: Efficient constraint algorithms for linked rigid bodies. *J. Comput. Chem.* **1998**, *19*, 102–111. [[CrossRef](#)]
48. Kräutler, V.; van Gunsteren, W.F.; Hünenberger, P.H. A fast SHAKE algorithm to solve distance constraint equations for small molecules in molecular dynamics simulations. *J. Comput. Chem.* **2001**, *22*, 501–508. [[CrossRef](#)]
49. Essmann, U.; Perera, L.; Berkowitz, M.L.; Darden, T.; Lee, H.; Pedersen, L.G. A smooth particle mesh ewald method. *J. Chem. Phys.* **1995**, *103*, 8577–8593. [[CrossRef](#)]
50. Bakan, A.; Meireles, L.M.; Bahar, I. ProDy: Protein dynamics inferred from theory and experiments. *Bioinformatics* **2011**, *27*, 1575–1577. [[CrossRef](#)]

Sample Availability: Samples of the compounds are not available from the authors.



© 2020 by the authors. Licensee MDPI, Basel, Switzerland. This article is an open access article distributed under the terms and conditions of the Creative Commons Attribution (CC BY) license (<http://creativecommons.org/licenses/by/4.0/>).